

# Initial-state and final-state vibrational effects in the treatment of molecular photoionization dynamics

Ivan Powis\*

*School of Chemistry, The University of Nottingham, University Park, Nottingham NG7 2RD, UK*

(Received 17 March 2011; published 6 July 2011)

The influence upon molecular photoionization dynamics of vibrational motion of the nuclei in both the initial (neutral) state and the final (molecular ion) state is examined using a consistent theoretical treatment applied to the wide range of existing experimental data for the benchmark CO C  $1s^{-1}$   $K$ -shell ionization. This allows comparisons to be made against cross sections, lab-frame  $\beta$ -parameter measurements, and molecule-frame photoelectron angular distributions that have all been recorded both with, and without, ion vibrational-state resolution. A relatively simple multiple-scattering treatment works well in all these applications, its performance comparing very favorably with alternative relaxed core Hartree-Fock methods. The calculations are extended to examine possible effects of vibrational excitation in the neutral, and show marked effects that extend to energies lying away from the obvious center of the CO  $\sigma^*$  shape resonance.

DOI: [10.1103/PhysRevA.84.013402](https://doi.org/10.1103/PhysRevA.84.013402)

PACS number(s): 33.80.Eh, 33.60.+q, 33.20.Wr

## I. INTRODUCTION

The importance of coupling between electronic and nuclear motions in electron-scattering and photoionization phenomena has long been recognized. This has been especially investigated in the vicinity of shape resonances, when a temporary trapping of the mobile electron promotes electron-molecule interaction. As a result, alongside the anticipated resonant cross-section enhancement, pronounced non-Franck-Condon final-state vibrational distributions are often encountered. Some of the very earliest full photoionization dynamics calculations drew attention to this, and showed how such vibrational effects could be incorporated into realistic modeling of the resonant cross sections,  $\sigma$ , and electron anisotropy parameters,  $\beta$  [1,2]. Nevertheless, the majority of calculations in the intervening few decades have been carried out in a fixed-nuclei approximation. Although frequently drawing on the generic qualitative lessons from these earlier calculations for discussion purposes, the additional computational effort was largely devoted to improving treatments of the purely electronic problem, including correlation effects.

Experimental developments, aided by the growing availability of tunable, polarized synchrotron radiation, have meanwhile provided a wealth of new data at vibrational resolution that demand the inclusion of nuclear motion for full understanding and insight. In recent years Poliakoff, Lucchese, and co-workers have provided a series of combined experimental-theoretical studies that fully examine vibrationally resolved, non-Franck-Condon, photoionization cross sections (vibrational branching ratios), and a seeming breakdown of symmetry selection rules, in a range of small molecular systems [3–7].

Another parallel experimental trend has been for the measurement of recoil-frame photoelectron angular distributions through the development of angle discriminating electron-ion coincidence detection techniques [8–15]. The molecule-frame photoelectron angular distributions (MF-PADs) that

can be inferred from such angle-resolving photoelectron-photoion coincidence (ARPEPICO) measurements provide, in principle, the most powerful probe of the photoionization dynamics, being sensitive to continuum electron phase shifts. Current ARPEPICO measurements are now starting to yield vibrationally resolved data, affording a fresh opportunity to investigate electron-nuclear coupling in photoionization.

Probably the most extensively studied system of vibrationally resolved MF-PADs is that of the carbon C  $1s$   $K$ -shell ionization of the CO molecule [16–19]. These results now complement an earlier investigation of the vibrationally resolved C  $1s^{-1}$  cross sections and  $\beta$  parameters [20]; similar data have also been obtained for the alternative O  $1s^{-1}$  photoionization of the same molecule [21,22].

The first photoionization calculations incorporating nuclear motion effects [1,2], referred to above, used the then-new continuum multiple-scattering treatment with  $X\alpha$  local-exchange potential (CMS- $X\alpha$ ) [23,24] to obtain electronic matrix elements. Since then, the use of more rigorous electronic treatments for small, symmetric molecules has become routine. Nevertheless, Cherepkov and co-workers have shown that, in the context of CO  $K$ -shell ionizations, a modified CMS- $X\alpha$  treatment proves to be at least as good as more sophisticated *ab initio* level relaxed core Hartree-Fock (RCHF) calculations for reproducing the detail of nonvibrationally resolved experimental MF-PADs [25,26].

One of the objectives of the present work is to show that this success of the CMS- $X\alpha$  method is maintained when it is extended to examine the vibrationally resolved CO data now available. A general advantage of the simple CMS- $X\alpha$  method is that it scales easily, permitting application to much bigger, low-symmetry systems. In particular, it is one of only two methods that have been applied to examine photoionization dynamics in nonsymmetric chiral molecules such as camphor (C<sub>10</sub>H<sub>16</sub>O) [27]. These systems are of growing interest as, when ionized with circularly polarized radiation, they display the phenomenon of photoelectron circular dichroism (PECD) [28]—a chiral asymmetry in the PAD from randomly oriented enantiomers that can be as large as 20%–32% [29–31]. The nature of the electron-scattering

\*ivan.powis@nottingham.ac.uk

dynamics in PECD further means that it is uniquely sensitive to chemical substitution and conformation changes, even when these may occur at some distance from the site of an initially localized orbital [28]. By the same token, one may anticipate an unprecedented sensitivity to nuclear vibrational motion even in nonresonant situations [32,33]. While extending the CMS- $X\alpha$  method to address vibrationally resolved PECD in large chiral molecules, it is useful to benchmark and validate the approach through application to a much simpler system, CO, and this is attempted here.

A secondary objective is to provide some realistic predictions of the likely variation of MF-PADs where vibrationally resolved *initial-state* ionization is concerned.<sup>1</sup> This seems especially pertinent given a growing trend to probe nonequilibrium reaction product populations created in time-resolved experiments via measurement of their MF-PADs [34–36]. The present model studies may offer some general guidance for the interpretation of MF-PAD data obtained from neutral species that may be vibrationally excited.

## II. METHOD

### A. Formalism

The formal inclusion of nuclear motion into the photoionization dynamics treatment is briefly recapped here, following approaches adopted by the groups of Lucchese [4] and Cherepkov [19]. Full electric dipole matrix elements for the photoionization can be written

$$D_{if} = \langle \Psi_f^{(-)} | \sum_j \hat{e} \cdot \mathbf{r}_j | \Psi_i \rangle. \quad (1)$$

In the adiabatic approximation the initial state,  $\Psi_i$ , can be expanded as  $\chi_{v''}''(Q)\psi_i(r; Q)$  and for the final state  $\Psi_f^{(-)} = \chi_{v^+}^+(Q)\psi_{f,\bar{k}}^{(-)}(r; Q)$  where the  $\chi_v(Q)$  are vibrational wave functions for quantum number  $v$  over the nuclear coordinates,  $Q$ . For the independent electron model  $\psi_i(r; Q)$  is the Born-Oppenheimer electronic wave function for the ionizing orbital with electron coordinates  $r$  and having a parametric dependence on  $Q$ . Similarly,  $\psi_{f,\bar{k}}^{(-)}(r; Q)$  is the appropriately normalized function for the continuum electron, momentum  $\mathbf{k}$ . Hence, the vibrationally resolved matrix element is

$$\begin{aligned} D_{if\bar{k}}^{v''v^+} &= \langle \chi_{v^+}^+(Q) \psi_{f,\bar{k}}^{(-)}(r; Q) | \hat{e} \cdot \mathbf{r} | \chi_{v''}''(Q) \psi_i(r; Q) \rangle, \\ &= \langle \chi_{v^+}^+(Q) | d_{if\bar{k}}(Q) | \chi_{v''}''(Q) \rangle, \end{aligned} \quad (2)$$

where  $d_{if\bar{k}}(Q)$  is the electronic matrix element for fixed nuclear geometry,  $Q$ . A subsidiary assumption made in the Franck-Condon approximation is that  $d_{if\bar{k}}(Q)$  is effectively constant for variations in  $Q$ , so that the electronic matrix element can be removed from the integration over  $Q$  implied in Eq. (2) and

$$D_{if\bar{k}}^{v''v^+} = d_{if\bar{k}} \int_0 \chi_{v^+}^+(Q) \chi_{v''}''(Q) dQ, \quad (3)$$

introducing the Franck-Condon factor as the integrated product of vibrational wave functions. If, however, invariance of electronic matrix element to change in the nuclear geometry is not to be assumed then Eq. (2) indicates the necessity to average  $d_{if\bar{k}}(Q)$  over the vibrational coordinate  $Q$ , weighted by the initial and final vibrational functions:

$$D_{if\bar{k}}^{v''v^+} = \int \chi_{v^+}^+(Q) d_{if\bar{k}}(Q) \chi_{v''}''(Q) dQ. \quad (4)$$

### B. Computational details

Electronic matrix elements,  $d_{if\bar{k}}(r_{CO})$ , were calculated for CO at selected internuclear separations,  $r_{CO}$ , by the CMS- $X\alpha$  method [23,24] using a potential constructed from overlapping atomic spheres that are enclosed in an outer spherical region. Atomic sphere radii were determined by the Norman procedure [37] with an empirically determined 0.80 scaling factor. This reduction from the usual default scaling of 0.88 [38,39] has the effect of increasing the net attractiveness of the model potential and was selected here to optimize alignment of the calculated shape resonance energy with the experimental cross-section data to better than 0.25 eV (see Discussion). The overlap of C and O atomic spheres then ranged from 45%, at the shortest internuclear distance treated, to 33% at the longest. The angular basis of spherical harmonic functions was truncated at  $\ell_{\max} = 4$  on the atomic spheres' centers,  $\ell_{\max} = 6$  in the outer sphere region; for the final state these limits were increased to  $\ell_{\max} = 6, 8$  respectively. Values of the statistical exchange parameter,  $\alpha$ , were taken from Schwarz [40].

The trial molecular potential, developed from the averaged atomic charge densities, was iterated to self-consistency following Slater's transition-state method [41] in which the occupation of the C  $1s$  orbital whose ionization was to be modeled was reduced by 0.5 electron. Once converged, the transition-state potential was modified in the asymptotic region to have the correct Coulombic potential for the separated ion plus photoelectron. The perturbation incurred by the initial levels as a result of this modification was assessed, and both the core  $1s$  orbital and the continuum function for a photoelectron  $\mathbf{k}$  were recalculated in this adapted transition-state potential, to allow the matrix elements  $d_{if\bar{k}}(r_{CO})$  to be evaluated. For this step the dipole operator was used in its acceleration form, having the advantage that the interstitial region then makes no contribution; this volume has in any case been minimized by the use of overlapping rather than touching atomic spheres.

The integration of  $d_{if\bar{k}}(r_{CO})$ , weighted by the product of neutral and ionic-state vibrational wave functions, to yield the vibrationally resolved  $D_{if\bar{k}}^{v''v^+}$  [Eq. (4)] was accomplished by a 21-point quadrature. Preliminary testing was performed to verify that this sampling of coordinate space  $r_{CO}$  gave reliable results from the integration step.

Interconversion between the experimental photon energy scale and the corresponding electron energies was accomplished using the adiabatic CO C  $1s^{-1}$  ionization potential (296.07 eV [42]) with appropriate allowance for any vibrational excitation being considered.

<sup>1</sup>Some of the preceding studies have considered vibrationally excited states of the ion, but only when generated from vibrationless ground-state neutrals.

### III. RESULTS

An overview of the fixed-nuclei calculations for cross sections and  $\beta$ -parameter curves that were obtained at the 21 discrete sampled geometries employed for the numerical integration of Eq. (4) is presented in Fig. 1. It is clearly evident that the  $\sigma^*$  shape resonance responds significantly to changes of the internuclear separation; the peak in the cross section becomes narrower and shifts to lower energy as the separation increases, as does the dip in the  $\beta$  parameter. This finding could be anticipated from earlier studies of shape resonances, including the original studies of  $N_2$  and  $O_2$  from Dehmer and Dill [1,2]. Evidently, as they pointed out, in such cases one needs to consider an appropriate average of the  $r_{CO}$  separations to fully explain experimental observations.

#### A. Nonresolved ion vibrational states

For data where the final ion vibrational state is *not resolved* this averaging can effectively be achieved by weighting the matrix element at each separation,  $r_{CO}$ , by the square of the initial neutral vibrational wave function,

$$D_{if\bar{k}}^{v''} = \int [\chi_v''(r_{CO})]^2 d_{if\bar{k}}(r_{CO}) dr_{CO}. \quad (5)$$

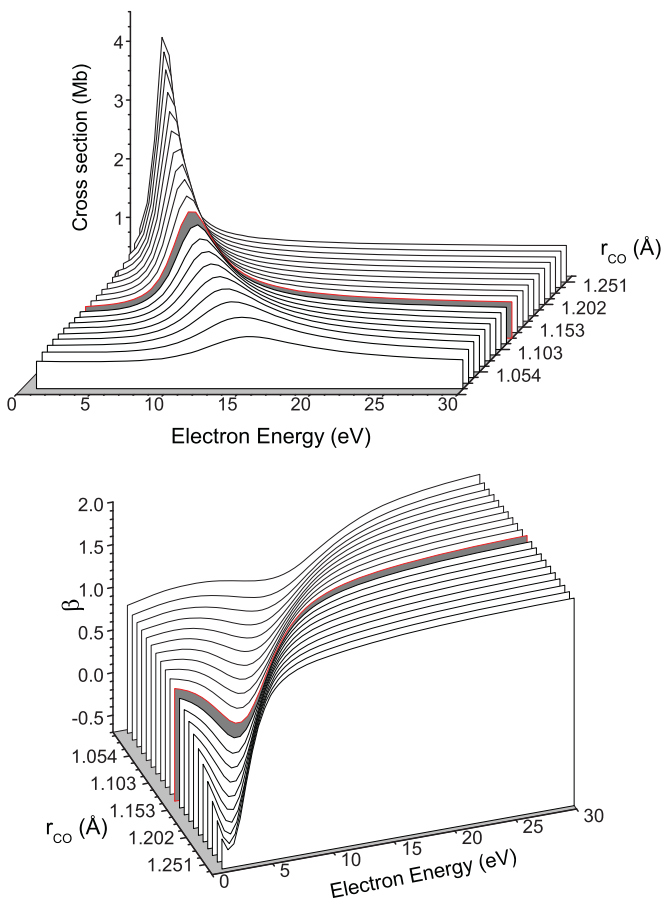


FIG. 1. (Color online) C  $1s^{-1}$  photoionization cross-section (top) and  $\beta$ -parameter (bottom) curves calculated for fixed internuclear separations,  $r_{CO}$ , that span the  $v'' = 0$  motion of CO. The curves at the equilibrium separation,  $r_e = 1.128$  Å, are distinguished by shading.

Assuming, then, the molecule to be ionized from its vibrational ground state, its wave function was generated using the well established vibrational parameters for the neutral CO molecule ( $\omega_e = 2169.81$   $\text{cm}^{-1}$ ,  $\omega_e x_e = 13.29$   $\text{cm}^{-1}$ ,  $r_e = 1.128$  Å; Ref. [43]). The initial dipole matrix elements were thus averaged according to Eq. (5) and used to obtain C  $1s^{-1}$  cross sections,  $\sigma$ , and angular distribution  $\beta$  parameters from threshold to well above the shape resonance region, as shown in Fig. 2. These calculations are compared to experimental data [20,44,45] in this figure. It should be noted that the narrow features observed experimentally in both  $\sigma$  and  $\beta$  around  $h\nu = 301$  eV are attributed to double-electron excitations [20,44], and are not therefore reproduced by any of the independent electron model treatments of the CO  $K$ -shell ionization discussed here or elsewhere in the literature.

Also included in Fig. 2 are the CMS- $X\alpha$  results from a fixed-geometry calculation at the equilibrium separation,  $r_e = 1.128$  Å. It is immediately apparent that the  $r_{CO}$ -averaged dipole matrix elements lead to a much improved quantitative agreement for the cross section, but a somewhat smaller improvement on the fixed-nuclei result is obtained for the  $\beta$  parameter.

Data sets such as those in Fig. 2 tend to focus attention on the reliability of the modeling of the shape resonance dynamics. Molecule-frame PADs, by contrast, provide richer dynamical information that allows a broader view to be

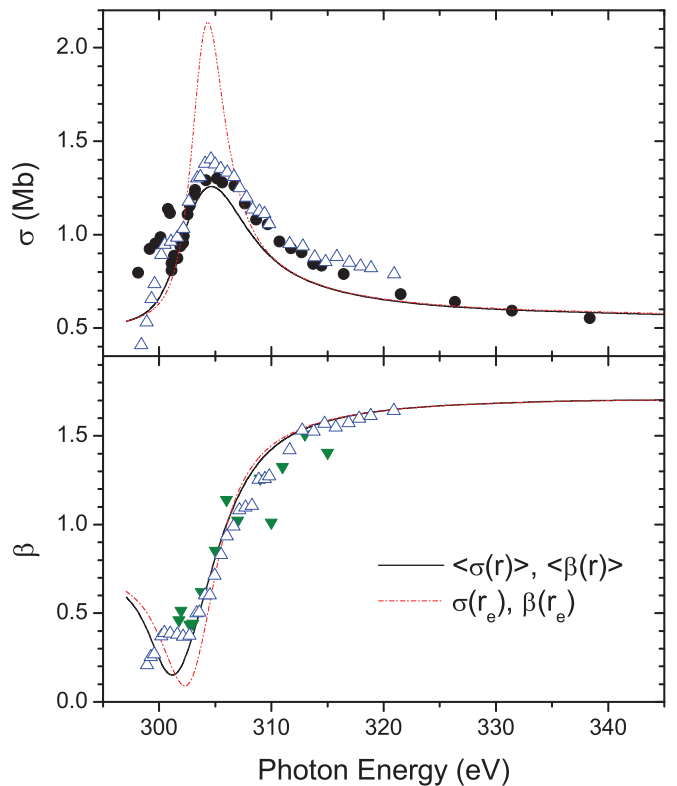


FIG. 2. (Color online) Cross-section (top) and  $\beta$ -parameter (bottom) curves for C  $1s^{-1}$  ionization to vibrationally unresolved  $CO^+$ . The CMS- $X\alpha$   $r_{CO}$ -averaged results (solid lines) are contrasted with the fixed-nuclei results for  $r_e = 1.128$  Å (broken lines). Experimental data taken from Ref [44] (open triangles); Ref. [20] (filled circles); Ref. [45] (filled inverted triangles).

taken. In Fig. 3 MF-PADs recorded with circularly polarized light at energies at, below, and above the  $\sigma^*$  resonance are presented. To facilitate visual comparison, the theoretical MF-PADs have been renormalized for plotting by a least-squares fitting optimization to the experimental data. The resulting  $\chi^2$  parameters also provide one possible criterion, or figure of merit, for judging performance of alternative theoretical models. The vibrationally averaged CMS-X $\alpha$  calculations are seen to be in overall good agreement with experiment [17,46], and perform very favorably in comparison to previous RCHF calculations [17,47], having significantly better  $\chi^2$  residuals at the four photon energies below the shape resonance. The  $h\nu = 300.7$  eV MF-PAD lies close to the region of double excitations, but nevertheless is well described by the present calculation. At the center of the  $\sigma^*$  resonance, 306.1 eV, the RCHF calculation performs rather better, while above this

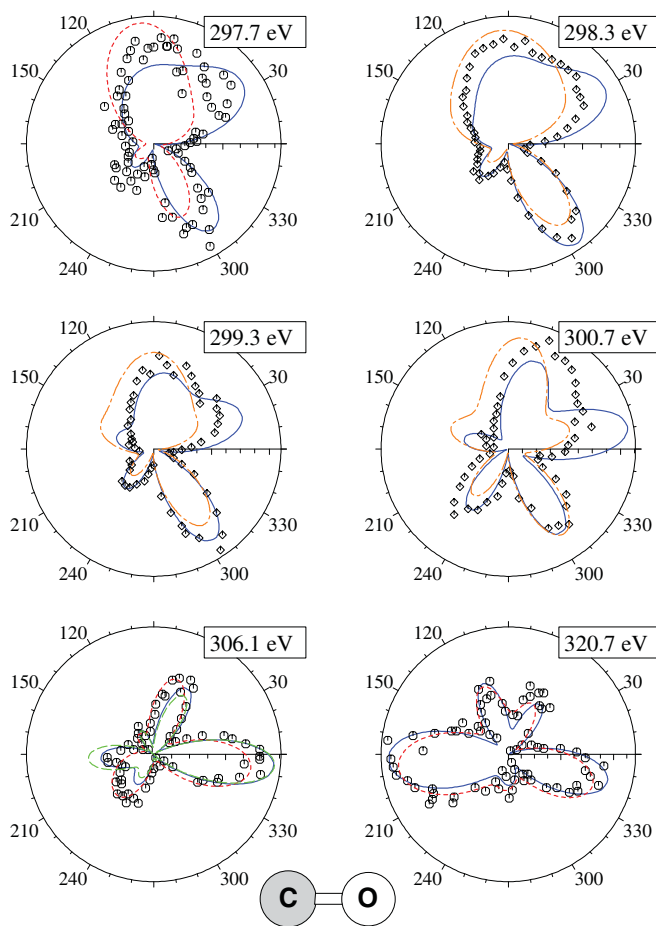


FIG. 3. (Color online) Fixed-molecule PADs for CO  $C 1s^{-1}$  photoionization to nonresolved ion vibrational states. The CO molecule is oriented as shown with the oxygen atom towards the right (at  $0^\circ$ ). Left-circularly polarized light, at the photon energies indicated, propagates into the plane of the page. Theoretical results: CMS-X $\alpha$  calculations (solid blue line), this work; fixed-nuclei ( $r_e$ ) RCHF(TS) calculations, Ref. [47] (red dotted line); RCHF calculations, Ref. [17] (orange dot-dashed line). Experimental data: from Ref. [46] (circles); from Ref. [17] (diamonds). For the shape resonance at 306.1 eV the PAD also includes a single, fixed-nuclei CMS-X $\alpha$  calculation at  $r_e$  (green dashed line). Each distribution is scaled for plotting to minimize its  $\chi^2$  residual with the experimental data.

region, at  $h\nu = 320.7$  eV, the two calculations and experiment are all in excellent agreement.

A comparison with fixed-nuclei CMS-X $\alpha$  calculations at  $r_e$  has also been made, but the results are omitted from Fig. 3 for clarity, as they do not differ significantly from the vibrationally averaged result. The one exception is for the 306.1-eV shape resonant MF-PAD where, as can be seen in the figure, the lobe lying to  $180^\circ$  is more extended in the fixed calculation at  $r_e$  than in either the vibrationally averaged or experimental data.

An alternative approach, or subsequent step, is investigation of the circular dichroism in the angular distribution (CDAD), defined as an asymmetry between the PADs,  $I(\theta)$ , measured with left- and right-circular polarizations:  $A_{CD}(\theta) = [I_{lcp}(\theta) - I_{rcp}(\theta)]/[I_{lcp}(\theta) + I_{rcp}(\theta)]$ . Figure 4 contains the available experimental CDAD results for the nonresolved  $C 1s^{-1}$  ion state, and the corresponding CMS-X $\alpha$  calculations for this property. The first experimental report [46] specifies the angular resolution on ion and electron detection, and RCHF calculations [47] (also shown in Fig. 4) were accordingly convoluted with an instrumental function for more direct comparison. In the present work a similar reasoning was applied, and so the CMS-X $\alpha$  results shown include integration over molecular orientations lying in a  $10^\circ$  cone, representing the finite experimental angular acceptance. The 298.3-eV CDAD data come from a later paper [17], albeit using the same apparatus, where the chosen angular acceptance is not specified. However, increasing the cone of molecular axes to  $17^\circ$  for the CMS-X $\alpha$  calculation provided a small, yet useful, further improvement in the experiment-theory fit. It seems probable that the single RCHF calculation presented for

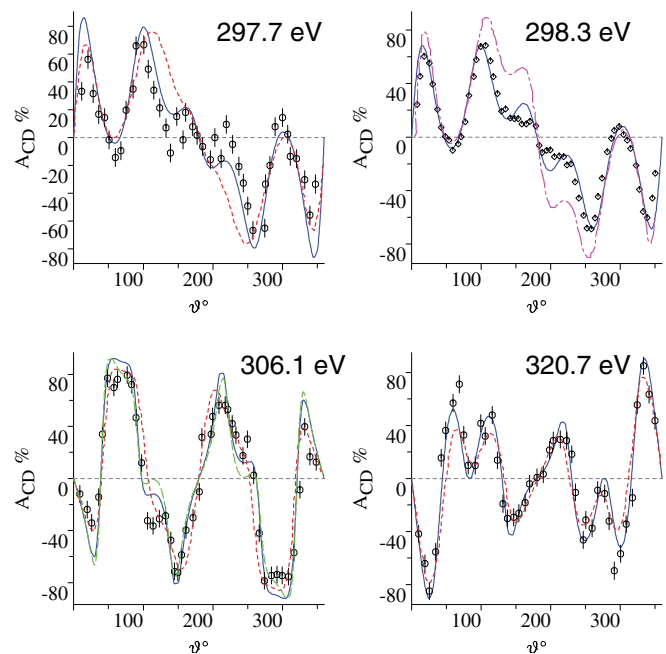


FIG. 4. (Color online) CDAD asymmetry factors,  $A_{CD}$ . The angle  $\theta$  is measured from the  $C \rightarrow O$  direction. Theoretical results: vibrationally averaged CMS-X $\alpha$  (blue solid line); fixed-nuclei ( $r_e$ ) CMS-X $\alpha$  (green dashed line, lower left panel); fixed-nuclei ( $r_e$ ) RCHF(TS) calculations, Ref. [47] (red dotted line); RCHF calculations, Ref. [17] (purple dot-dashed line). Experimental data: from Ref. [46] (circles); from Ref. [17] (diamonds).

298.3 eV [17] makes no allowance for an instrument function. While the fit with experiment is worse than any of the other calculated curves in Fig. 4, the discrepancy is far larger than the changes brought about by the inclusion of such a treatment for the raw CMS- $X\alpha$  results.

Fixed-nuclei calculations at  $r_e$  were also compared with the vibrationally averaged CMS- $X\alpha$  CDAD results. Negligible differences were noted, except for at the  $\sigma^*$  resonance (306.1 eV) where a minor degradation, a slightly more peaked profile, was evident. These are, therefore, again omitted from the figure.

### B. Resolved ion vibrational states

Several determinations for the  $\text{CO}^+ \text{C } 1s^{-1}$  state vibrational parameters have been reported [20,48–51]. These reports proceed by a Franck-Condon fitting exercise to the above-threshold vibrational intensity patterns observed in the high-resolution x-ray photoelectron spectrum (XPS), and are agreed on a shortening of the bond length in the core ionized state. The ion vibrational wave functions derived from these various parameter sets have all been fully evaluated in calculations made with  $r_{\text{CO}}$  averaged CMS- $X\alpha$  matrix elements, Eq. (4), and vibrationally resolved cross sections are compared with experiment in Fig. 5. The earlier harmonic oscillator fits [20,48] performed significantly less well overall than the anharmonic Morse potential models [49–51], while for the latter, the best experimental agreement obtained in Fig. 5 is achieved with the parameters reported by Matsumoto *et al.* [51]

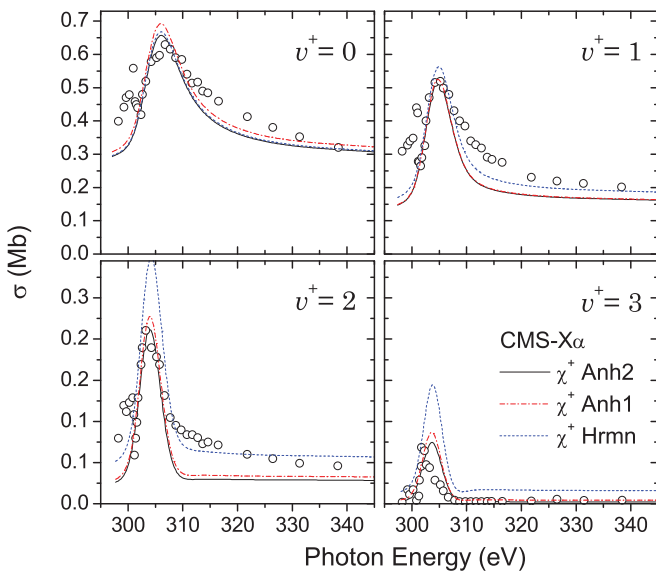


FIG. 5. (Color online) CMS- $X\alpha$  calculated cross sections for  $\text{C } 1s^{-1}$  ionization to vibrationally resolved  $\text{CO}^+$ . A  $v^+ = 0$  anharmonic vibrational wave function (Ref. [43]) was used for the neutral state in all these calculations. For the  $\text{CO}^+$  ion, anharmonic vibrational wave functions,  $\chi^+$ , were evaluated using parameters ( $r_e, \omega_e, \omega_e x_e$ ) from either Ref. [49] (curves labeled Anh1) or from Ref. [51] (curves labeled Anh2); harmonic oscillator ion wave functions ( $r_e, \omega_e$  from Ref. [48]) were employed for the curves labeled Hrmn. Experimental data (circles) taken from Ref. [20]. Note the change in vertical scale between top and bottom row.

( $\omega_e = 2479.0 \text{ cm}^{-1}$ ,  $\omega_e x_e = 23 \text{ cm}^{-1}$ ,  $r_e = 1.077 \text{ \AA}$ ). It may be noted that these authors specifically argue the need to apply the Franck-Condon analysis surprisingly far above the shape resonance energy—in this case  $\geq 80 \text{ eV}$  from threshold—evidently with some justification.

A similar comparison of vibrationally resolved experimental and calculated  $\beta$  parameters is presented in Fig. 6. Differences between the alternative anharmonic parameter sets are here less pronounced, and the agreement with experiment is again very good (noting as before that the double excitation features at  $\sim 301 \text{ eV}$  in both Figs. 5 and 6 are excluded from these theoretical treatments).

Anticipating the MF-PAD results that will follow, the differences between the various vibrational parameter sets were here less pronounced than was evident in the cross-section data and, indeed, largely insignificant. Nevertheless, because of the superior intensities obtained in Fig. 5, the Matsumoto parameters [51] will be used for the ion vibrational state in the CMS- $X\alpha$  calculations that follow.

Figure 7 compares CMS- $X\alpha$  calculations for specific ion vibrational levels with experimental MF-PADs for the case of linear polarization parallel to the molecular axis [16], while a similar comparison with experimental MF-PADs obtained using circular polarization [17] is provided in Fig. 8. In both cases the CMS- $X\alpha$  results capture the variation in the experimental MF-PADs seen with both increasing photon energy and ion vibrational state. This is so even for the 300.7-eV PADs recorded with circular polarization, which may be affected by the double excitations expected around this photon energy, and not therefore covered by the theoretical model.

As before, CDAD measurements provide an alternative perspective from which to consider the ionization with circular polarization, and Fig. 9 shows the 298.3eV CDAD asymmetries for the resolved ion vibrational states  $v^+ = 0, 1, 2$ , comparing the CMS- $X\alpha$  results with RCHF

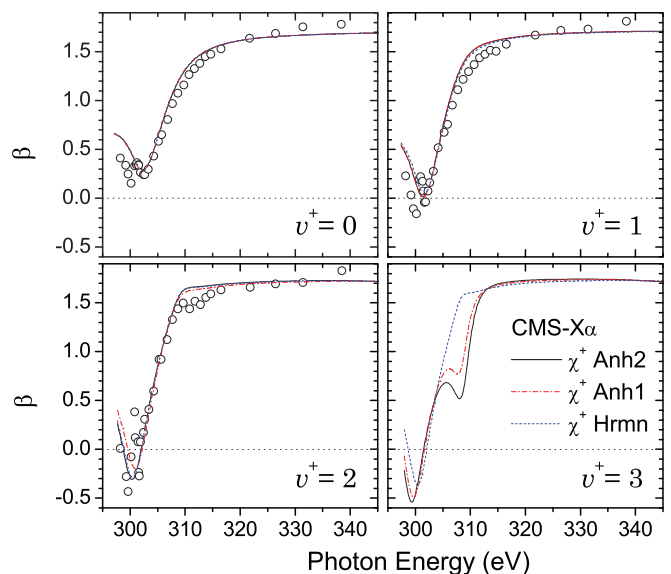


FIG. 6. (Color online) CMS- $X\alpha$  calculated  $\beta$ -parameter curves for  $\text{C } 1s^{-1}$  ionization to vibrationally resolved  $\text{CO}^+$ . Details as for Fig. 5.

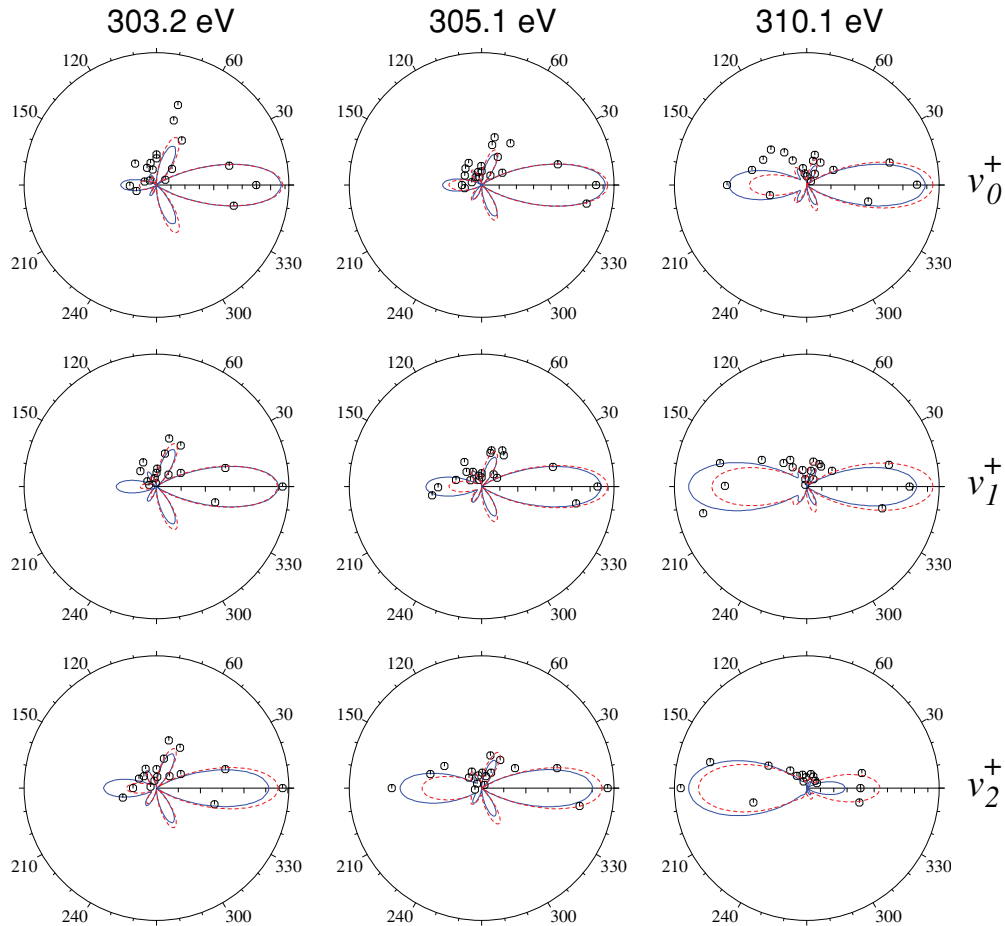


FIG. 7. (Color online) Molecule-frame PADs for resolved ion vibrational states. The linear polarization and the CO molecule are both aligned along the horizontal axis (with the O atom to the right, pointing at  $0^\circ$ ): CMS- $X\alpha$  calculations, this work (blue solid line); RCHF calculations, Ref. [16] (red dotted line). Experimental data also from Ref. [16]. Theoretical distributions have been scaled to minimize their  $\chi^2$  residual with the corresponding experimental data before plotting.

calculations and experiment [17]. Presented in this fashion, the better quantitative performance of the current calculation is more evident. CDAD in some senses facilitates and enhances theory-experiment comparisons because of (i) the inherent normalization of the signal, and (ii) the ability to suppress purely instrumental asymmetries (such as detector gain inhomogeneities) through forming a difference (dichroism) signal. As discussed previously, it is reasonable to suppose that a finite angular acceptance in the experiment may create some smearing of the data. The results of simulating this by allowing any molecular orientation tilted into a  $17^\circ$  cone are included in Fig. 9. While the CMS- $X\alpha$  fit to experiment is slightly improved by this smearing, the changes are small and it appears unlikely that the omission of instrumental effects accounts for the bigger discrepancies of the RCHF calculation.

### C. Vibrationally excited neutral state ionization

The influence of different initial vibrational states of the neutral molecule can also be examined within this model. Inevitably, one expects to find changes in the calculated cross sections due to the different Franck-Condon factors that pertain

even when well removed from a shape resonance—and much more dramatic variations can be anticipated in the vicinity of a shape resonance.

Figure 10 provides some example, fully resolved  $v'' \rightarrow v^+$  MF-PADs for the C  $1s^{-1}$  photoionization with parallel linear polarization. To provide a reference, experimental data for the  $v'' = 0$  ionization are also included, and these then highlight how misleading a comparison might be if the vibrational levels involved have not been fully identified. The parallel linear polarization tends to produce a PAD that is oriented along the internuclear axis. Results for the  $v^+ = 1$  level, around the  $\sigma^*$  shape resonance some 8–10 eV above threshold, show a clear forward-backward orientation, but with a preponderance in opposite directions for the  $v'' = 0, 2$  and  $v'' = 1$  initial vibrational states. Similar, equally prominent discrepancies in the predicted orientations for the different  $v''$  levels are seen for other examples in this figure, lying to high and low energy of the shape resonance.

The very evident strong influence of both initial and final vibrational state on the shape of the expected MF-PAD may not be so surprising at the shape resonance, because of the known propensity for strong electron-nuclei coupling in such

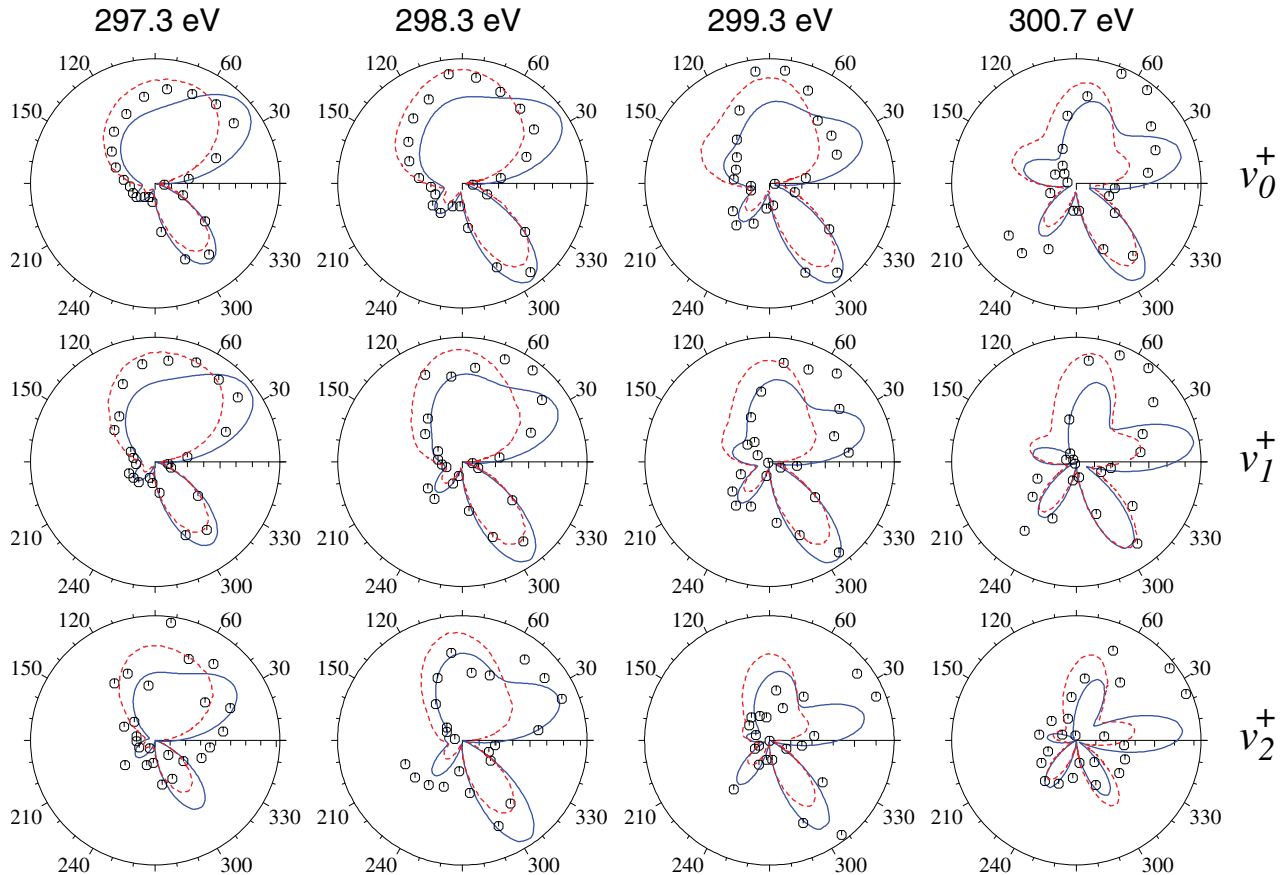


FIG. 8. (Color online) C  $1s^{-1}$  MF-PADs for left-circularly polarized radiation (at indicated photon energies, below the shape resonance) propagating into the plane of the page. The CO molecule is aligned horizontally, O atom to the right. Each row shows data for a resolved ion vibrational state. CMS- $X\alpha$  calculations (blue solid line); experimental data (circles), and RCHF calculations (red dotted line), both from Ref. [17]. Theoretical distributions have been scaled to minimize their  $\chi^2$  residual with the corresponding experimental data before plotting.

a circumstance. Figure 11 provides further results for fully vibrationally resolved MF-PADs, this time corresponding to ionization by circularly polarized light, at a series of energies that all fall below the shape resonance region. Again, experimental results for the  $\nu'' = 0$  ionization are included as a point of reference for comparing the CMS- $X\alpha$  calculations. Some interesting trends may be discerned. For the ionization to  $\nu^+ = 0$  and  $\nu^+ = 1$  the assumed initial level,  $\nu''$ , seems to have little impact at the lowest electron energies around 1 eV, though this increases above  $\sim 3$  eV. This might appear a little counterintuitive, since the photoelectron would be expected to have most sensitivity to vibrational motion of the ion core when emerging most slowly, but perhaps is indicative of the reach of shape resonance dynamics down into this seemingly nonresonant region.

In apparent contrast the  $\nu'' = 0, 1$  and  $\nu'' = 2$  circular polarization MF-PADS are distinctively different at the lowest electron energies, but are perhaps rather more similar at  $\sim 4$  eV.

#### IV. DISCUSSION

The range and quality of the experimental data available for the CO C  $1s^{-1}$  photoionization has increased significantly in recent years. The theoretical treatments that have accompanied this progress have nearly all been performed using a relaxed

core Hartree-Fock (RCHF) approach [14,16–19,47], and have generally shown significant improvements over earlier treatments—when such comparisons may be made. However, it has been demonstrated that the older CMS- $X\alpha$  method, adapted to use more realistic partitioning of the potential, can perform at least as well as these RCHF approaches for description of CO O  $1s^{-1}$  and C  $1s^{-1}$  nonvibrationally resolved, linear polarization MF-PADs in the fixed-nuclei approximation [25,26,52]. The present work corroborates and extends this favorable comparison.

Both CMS- $X\alpha$  and RCHF are independent electron treatments. The validity of relying on this approximation for the CO K-shell ionizations has been justified by random phase approximation (RPA) calculations that demonstrate many-electron correlation effects to be negligible [18,25]. With a primary assumption thus satisfied, this creates a favorable situation, allowing a fair comparison of the performance of the relatively simple CMS- $X\alpha$  method with the RCHF approaches and with experiment in this particular system.

A generic difficulty for calculating the continuum electron functions lies in securing a potential with the correct attractiveness, such that the electron energy scale matches experiment. This problem is most apparent in comparison with experimental cross-section and  $\beta$ -parameter curves, where the

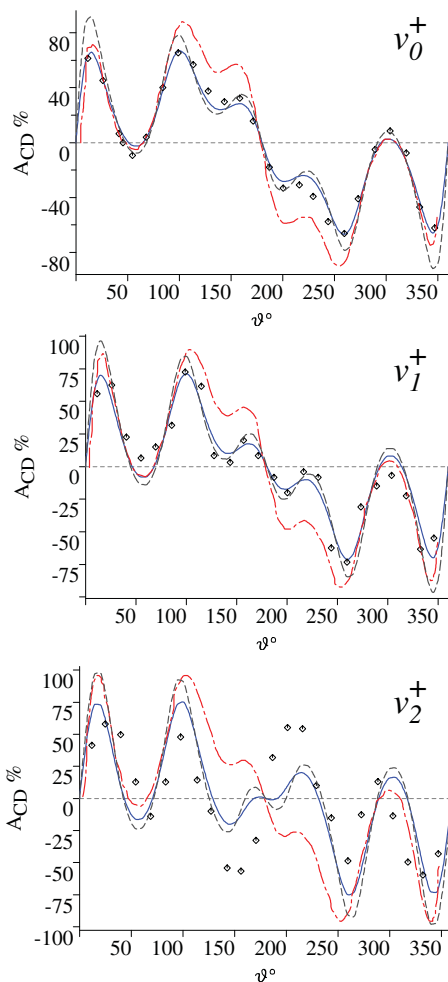


FIG. 9. (Color online) CDAD asymmetry,  $A_{CD}$ , at  $h\nu=298.3$  eV for resolved  $v_{0,1,2}^+$  vibrational levels of  $\text{CO}^+$ . CMS- $X\alpha$  calculations before (gray dashed line) and after (blue solid line) allowance for finite angular acceptance in the experiment. Experimental data (diamonds) and RCHF calculations (orange dot-dashed line) are from Ref. [17].

energy of resonant continuum features may appear displaced; it would be less immediately obvious when comparing, e.g., MF-PADs, at one or more fixed photon energies. The simultaneous comparison, as offered here, of a single model's results for  $\sigma$ ,  $\beta$  curves (i.e., as continuous functions of energy) alongside the more detailed angular distributions that have been obtained, but for just a few discrete energies, allows a better opportunity to assess whether the MF-PAD models may be compromised by inaccurately reproduced binding energies. A pragmatic solution to such difficulties is sometimes to apply *post hoc* an offset to the electron energy scale, although the limitations for this are obvious and some attempt to improve the physical approximations would be preferred.

The original formulation of the RCHF method [53] called for calculation of the continuum wave function in the potential of a variationally reoptimized ( $N-1$ )-electron core state—allowing for the relaxation and screening of the core hole by the remaining electrons. Experience shows, however, that the relaxation effects tend to be overestimated by this approach. A subsequent modification [14,47]—which we here denote RCHF(TS)—adopted Slater's transition-state method [41], in

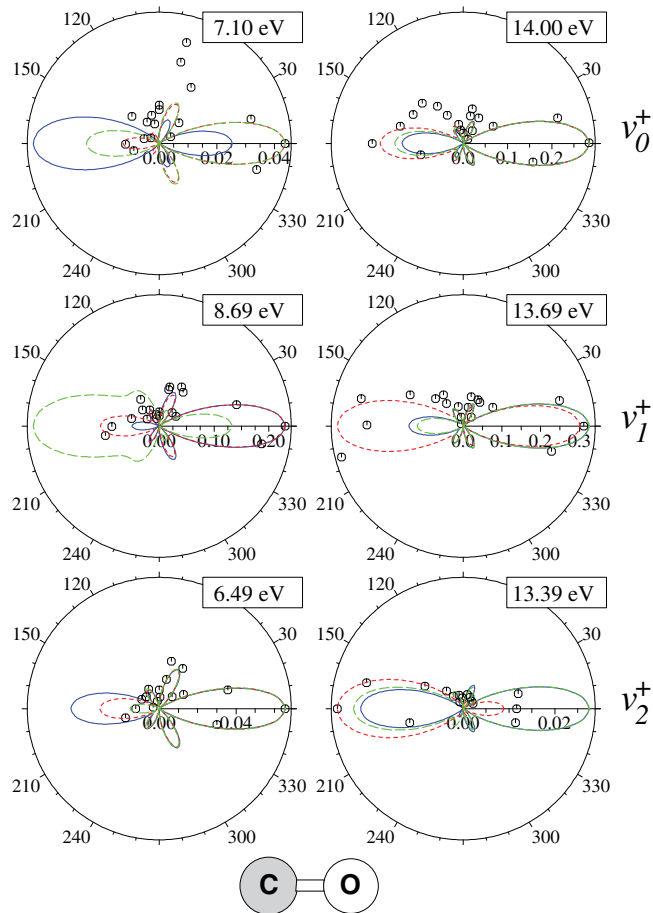


FIG. 10. (Color online) CMS- $X\alpha$  calculated MF-PADs for CO  $\text{C } 1s^{-1}$  ionization by linearly polarized light aligned parallel to the molecular axis (shown) and from neutral states having  $v'' = 2$  (blue solid line);  $v'' = 1$  (green dashed line);  $v'' = 0$  (red dotted line). Calculations are at the indicated electron kinetic energies and for ionization to the  $v^+ = 0, 1, 2$  states in the top, middle, and bottom rows, respectively. For reference the experimental data for  $v'' = 0$  ionization (Ref [16]) are also included (circles). All PADs are normalized to the peak in the  $v'' = 2$  calculation to emphasize comparison of their shapes.

which orthogonal initial- and final-state orbitals are calculated in the same, self-consistent potential with a half-electron core hole vacancy. This is exactly the approach used for the CMS- $X\alpha$  calculations here. It is worth noting that Slater introduced the transition state with a  $1\frac{1}{2}$  electron orbital occupancy by showing that it satisfies the condition for the orbital eigenvalue in the  $X\alpha$  local-exchange potential to equal, to better than second order, the ionization energy [41]. One can, however, understand how this half-ionized transition state may reproduce the twin effects of an increased binding energy, due to the core hole charge, balanced by its partial screening by relaxation of the remaining electrons.

Use of the transition-state potential for the present CMS- $X\alpha$  calculations provided a very significant improvement over that of the  $N$ -electron CO molecule. A further fine tuning, of up to  $\sim 0.5$  eV, was finally performed by varying the atomic sphere radii (specifically the reduction factor applied to the Norman sphere sizes [37]), until the position of the calculated shape

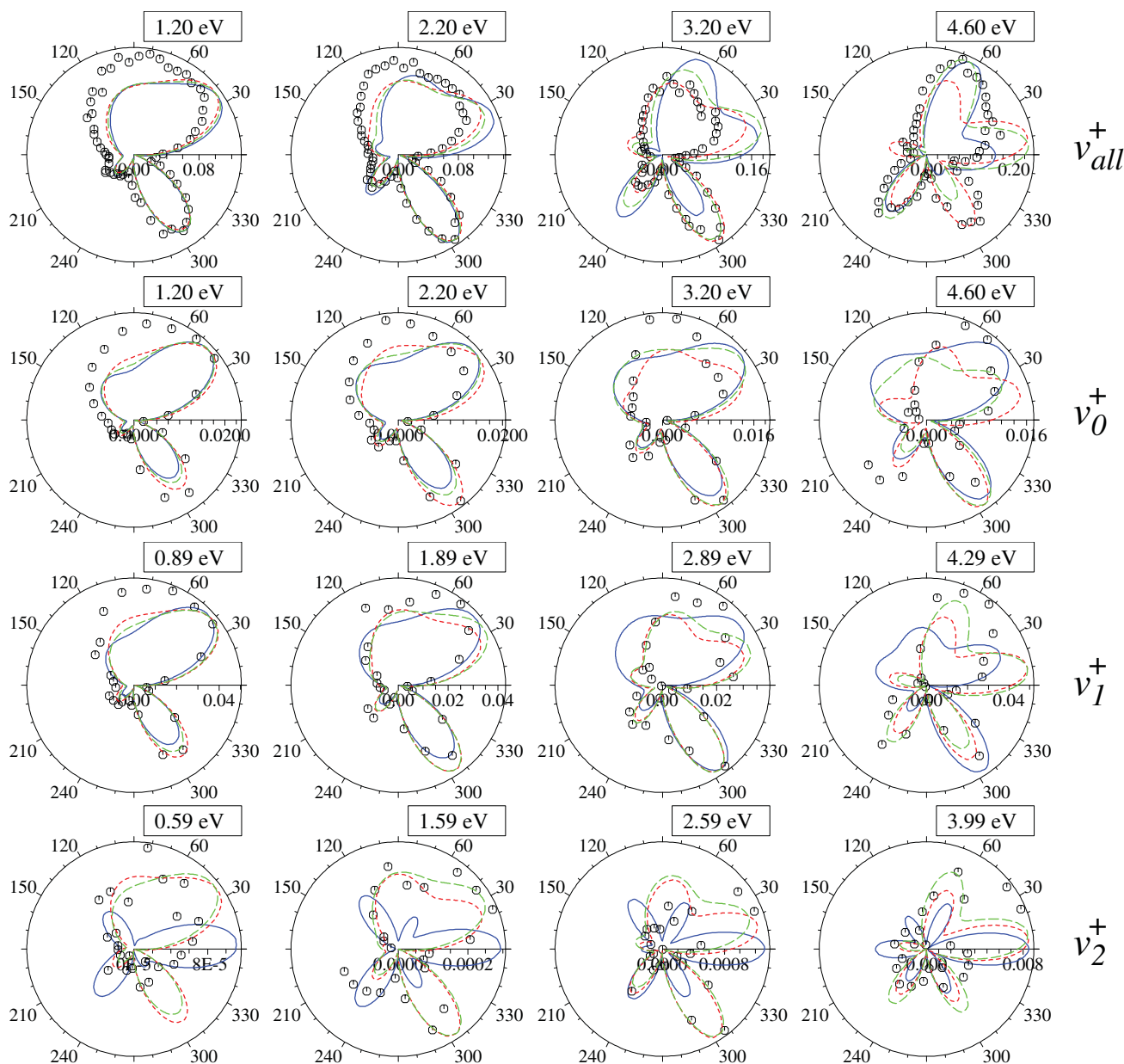


FIG. 11. (Color online) CMS-X $\alpha$  MF-PADs for ionization by left-circularly polarized light propagating into the plane of the page and from neutral CO having  $\nu'' = 2$  (blue solid line);  $\nu'' = 1$  (green dashed line);  $\nu'' = 0$  (red dotted line). Experimental data for the  $\nu'' = 0$  ionization (Ref. [17]) are included as a reference. The top row shows data for nonresolved ion vibrational levels, the rows beneath are for the indicated ion vibrational level, and are at the indicated electron kinetic energies. All distributions are normalized to the peak in the  $\nu'' = 2$  calculation.

resonance best aligned with experiment, as viewed in Fig. 2. All subsequent CMS-X $\alpha$  calculations presented here used this parametrization.

In studies of the CO  $1s^{-1}$  photoionization it was found that while RCHF calculations generated a 2-eV offset in the calculated continuum energy scale [16], a 3–4-eV offset was still being inferred for RCHF(TS) calculations [14,26]. Consequently, in a further modification of the RCHF method, Cherepkov and co-workers [18] have introduced the use of a fractional core hole charge,  $z_e$ , that is treated as an adjustable parameter. At the same time the restriction requiring orthogonal orbitals was also relaxed. Initial and final states are thus calculated in more physically appropriate potentials.

When applied for the calculation of CO  $K$ -shell cross sections and  $\beta$  parameters, the optimal value of the parameter  $z_e$  was found to be somewhat dependent on the exact property being calculated [18,25]. This revised RCHF method does not, however, appear to have been applied to the calculation of MF-PADs.

When the earlier RCHF variants are applied to reproduce the nonvibrationally resolved CDAD data (Fig. 4) or the MF-PADs obtained with circular polarization (Fig. 3), RCHF calculations that assume a fully depleted core hole potential [17] appear to perform rather less well than do the RCHF(TS) calculations [47] even though the latter calculations are carried through only in the fixed-nuclei approximations at  $r_e$ .

Moreover, the present CMS- $X\alpha$  calculations for these MF-PADs perform at least as well as, and for the CDAD are better than, either RCHF calculation. These differences are not necessarily associated with averaging over the initial-state vibrational motion. Except as noted in the Results section, the inclusion of vibrational averaging in the CMS- $X\alpha$  calculations was found to provide little advantage when attempting to reproduce data for the nonvibrationally resolved  $\text{CO}^+$  ionization. From the preceding discussion, the difficulty here for the RCHF calculations may lie in fixing the energy scale in the continuum, a problem alluded to but not fully resolved in Ref. [47]. The same problem was clearly noted in the closely related RCHF (full hole potential) calculations [16] for the vibrationally resolved  $\text{CO}^+$  linearly polarized MF-PADs (Fig. 7), where a 2-eV offset was applied to align the calculated and experimental shape resonance positions in the calculated cross sections. Nevertheless, the vibrationally resolved MF-PADs of Fig. 7 are well reproduced in both CMS- $X\alpha$  and RCHF calculations. Although some differences are evident, the  $\chi^2$  parameters from the scaling to experiment indicate little to choose between the two methods in the case of  $v_{0,1}^+$ , with a slight preference for the RCHF calculations for  $v_2^+$ .

The agreement between *either* of these calculations and experiment, while still convincing, is perhaps a little less quantitative for the circular polarization MF-PADS (Fig. 8). Neither calculation performs consistently better than the other as judged from the  $\chi^2$  fit statistics, perhaps reflecting a degree of uncertainty in the challenging experimental measurements. However, when a visual comparison is made for the corresponding, vibrationally resolved CDAD curves (Fig. 9) the CMS- $X\alpha$  results clearly are the more quantitatively reliable.

The treatment applied here for *nonresolved* ion vibrational-state data, using Eq. (5), effectively amounts to averaging over the initial vibrational motion (i.e., the zero-point motion for the case when  $v'' = 0$ ); because the matrix elements  $d_{i\bar{f}\bar{k}}(Q)$  are weighted by the square of the initial vibrational wave function,  $[\chi_v''(Q)]^2$ , there is no phase information. Conversely, when a specific excited vibrational level in the ion is considered, using Eq. (4), the vibrational overlap,  $\chi_{v^+}^+(Q)\chi_{v''}''(Q)$ , that now appears introduces a phase that varies across the vibrational potential. Qualitatively, one may observe from Fig. 11 that the calculations for the nonresolved ion state show the least variation with assumed neutral vibrational state; those made for resolved ion vibrations, and especially for  $v^+ = 2$ , display much more variability. Looking down the columns in Fig. 11 it is difficult to spot intuitively how the calculations made for specific ion vibrational levels reached from, for example,  $v'' = 2$  would combine to yield the nonresolved MF-PAD in the top row, even allowing for the reducing vibrational branching ratio that may be anticipated. At this level of detail it can be inferred that the vibrational phase becomes important.

Although there are currently no experimental data with which to make comparison, the fully vibrationally resolved MF-PAD calculations that are presented in Figs. 10 and 11 are very striking, showing that at this level of resolution very significant differences emerge, depending on vibrational states, and that these large effects are not simply confined to

the immediate vicinity of the shape resonance in the  $\text{CO}^+$  ionization. It is clearly impossible to make meaningful inferences about molecular orientation (as opposed to alignment) simply from an observed forward-backward imbalance in the molecular-frame PAD without recourse to a full photoionization dynamics calculation to include resonance and vibrational effects, a conclusion that may be pertinent if photoelectron spectroscopy is to be used to probe nonequilibrium samples, e.g., molecular dissociation fragments. Equally, this suggests that at some level care may be required if larger systems that could have thermally excited vibrational modes are to be examined. Although the experience here appears to confirm that, in the absence of ion vibrational-state resolution, a fixed-nuclei calculation may prove sufficient for many purposes, the introduction of such low-frequency modes (which are also likely to be large-amplitude vibrations), combined with the phase changes between inner and outer regions of the potential that would be implied by a  $v'' \neq 0$  wave function could render this assumption less valid.

## V. SUMMARY

Using a single free parameter to obtain a potential that matches the calculated and experimental energies of the  $\sigma^*$  shape resonance in the C  $1s^{-1}$  photoionization, a consistent theoretical treatment that makes full allowance for vibrational motion, and that covers at once the full range of available experimental data on this system— $\sigma$  and  $\beta$ -parameter curves as a function of photon energy, MF-PADs in linear and circular polarization, and CDAD asymmetries; all with and without ion vibrational-state resolution—has been achieved. This has been further applied to consider the likely effects of photoionization from vibrationally state-selected neutral CO molecules, representing a situation which one may anticipate will become more common as experimental methods and applications develop.

While the known importance of incorporation of vibrational motion in fixing the width and intensity of shape resonance features is confirmed, a comparison of nonvibrational-state-resolved photoelectron angular distributions, measured in non-resonant energy regions, indicates that vibrationally averaged calculations differ little from simpler fixed-nuclei calculations performed at the equilibrium geometry—thus providing a *post hoc* justification for the very many fixed-nuclei calculations reported. At a shape-resonant energy, however, the vibrational averaging appears to offer a definite, though small, improvement in calculated PADs.

Perhaps unsurprisingly, these conclusions change when ion vibrational-state-resolved PADs are considered. Experimentally these show a very significant variation with ion vibrational level, and these changes are well reproduced by the full CMS- $X\alpha$  calculations that are presented here. The comparisons that are made with various RCHF calculations show that, across the range of data for this system, the CMS- $X\alpha$  method is capable of reproducing the experimental results at least as well as do the RCHF calculations, corroborating a previous judgment based on a more restricted examination of fixed-nuclei PAD calculations [25,26]. A possible advantage here of the simpler CMS- $X\alpha$  approach is that care has been taken to generate a potential which has a realistic attraction, such that the

continuum energy scale is quantitatively accurate, before any attempt to examine PADs, etc., at discrete energies. Another advantage, particularly for future extensions, is that the integration over nuclear coordinates is relatively undemanding from a computational perspective in this approximation.

The comparative success of the vibrationally adapted CMS- $X\alpha$  method in this simple, well studied case should help validate its use for other more challenging applications to the photoionization of much larger systems that are currently beyond the scope of more *ab initio* methods.

- 
- [1] J. L. Dehmer, D. Dill, and S. Wallace, *Phys. Rev. Lett.* **43**, 1005 (1979).
- [2] P. M. Dittman, D. Dill, and J. L. Dehmer, *J. Chem. Phys.* **76**, 5703 (1982).
- [3] G. J. Rathbone, E. D. Poliakoff, J. D. Bozek, and R. R. Lucchese, *Phys. Rev. Lett.* **92**, 143002 (2004).
- [4] E. D. Poliakoff and R. R. Lucchese, *Phys. Scr.* **74**, C71 (2006).
- [5] A. Das, J. S. Miller, E. D. Poliakoff, R. R. Lucchese, and J. D. Bozek, *J. Chem. Phys.* **127**, 044312 (2007).
- [6] R. R. Lucchese, J. D. Bozek, A. Das, and E. D. Poliakoff, *J. Chem. Phys.* **131**, 044311 (2009).
- [7] A. Das, E. D. Poliakoff, R. R. Lucchese, and J. D. Bozek, *J. Chem. Phys.* **130**, 044302 (2009).
- [8] K. G. Low, P. D. Hampton, and I. Powis, *Chem. Phys.* **100**, 401 (1985).
- [9] A. V. Golovin, N. A. Cherepkov, and V. V. Kuznetsov, *Z. Phys. D* **24**, 371 (1992).
- [10] E. Shigemasa, J. Adachi, M. Oura, and A. Yagishita, *Phys. Rev. Lett.* **74**, 359 (1995).
- [11] I. Powis, *J. Chem. Phys.* **99**, 3436 (1993).
- [12] F. Heiser, O. Gessner, U. Hergenhahn, J. Vieffhaus, K. Wieliczek, N. Saito, and U. Becker, *J. Electron Spectrosc. Relat. Phenom.* **79**, 415 (1996).
- [13] P. Downie and I. Powis, *J. Chem. Phys.* **111**, 4535 (1999).
- [14] S. Motoki, J. Adachi, Y. Hikosaka, K. Ito, M. Sano, K. Soejima, A. Yagishita, G. Raseev, and N. A. Cherepkov, *J. Phys. B* **33**, 4193 (2000).
- [15] T. Weber *et al.*, *J. Phys. B* **34**, 3669 (2001).
- [16] J. Adachi, K. Hosaka, S. Furuya, K. Soejima, M. Takahashi, A. Yagishita, S. K. Semenov, and N. A. Cherepkov, *Phys. Rev. Lett.* **91**, 163001 (2003).
- [17] T. Jahnke *et al.*, *Phys. Rev. Lett.* **93**, 083002 (2004).
- [18] S. K. Semenov, N. A. Cherepkov, T. Jahnke, and R. Dorner, *J. Phys. B* **37**, 1331 (2004).
- [19] N. A. Cherepkov and S. K. Semenov, *Int. J. Quantum Chem.* **107**, 2889 (2007).
- [20] H. M. Köppe, A. L. D. Kilcoyne, J. Feldhaus, and A. M. Bradshaw, *J. Electron Spectrosc. Relat. Phenom.* **75**, 97 (1995).
- [21] D. A. Mistrov, A. De Fanis, M. Kitajima, M. Hoshino, H. Shindo, T. Tanaka, Y. Tamenori, H. Tanaka, A. A. Pavlychev, and K. Ueda, *Phys. Rev. A* **68**, 022508 (2003).
- [22] S. K. Semenov, N. A. Cherepkov, A. De Fanis, Y. Tamenori, M. Kitajima, H. Tanaka, and K. Ueda, *Phys. Rev. A* **70**, 052504 (2004).
- [23] D. Dill and J. L. Dehmer, *J. Chem. Phys.* **61**, 692 (1974).
- [24] J. W. Davenport, *Phys. Rev. Lett.* **36**, 945 (1976).
- [25] N. A. Cherepkov, S. K. Semenov, A. V. Golovin, J. Adachi, and A. Yagishita, *J. Phys. B* **37**, 4803 (2004).
- [26] A. V. Golovin and N. A. Cherepkov, *J. Phys. B* **35**, 3191 (2002).
- [27] M. Stener, D. D. Tommaso, G. Fronzoni, P. Decleva, and I. Powis, *J. Chem. Phys.* **124**, 024326 (2006).
- [28] I. Powis, in *Advances in Chemical Physics*, edited by J. C. Light (Wiley, New York, 2008), Vol. 138, p. 267.
- [29] S. Stranges *et al.*, *J. Chem. Phys.* **122**, 244303 (2005).
- [30] V. Ulrich, S. Barth, S. Joshi, U. Hergenhahn, E. A. Mikajlo, C. J. Harding, and I. Powis, *J. Phys. Chem. A* **112**, 3544 (2008).
- [31] S. Daly, I. Powis, G. A. Garcia, H. Soldi-Lose, and L. Nahon, *J. Chem. Phys.* **134**, 064306 (2011).
- [32] G. Contini, N. Zema, S. Turchini, D. Catone, T. Prosperi, V. Carravetta, P. Bolognesi, L. Avaldi, and V. Feyer, *J. Chem. Phys.* **127**, 124310 (2007).
- [33] G. Garcia, L. Nahon, S. Daly, and I. Powis (unpublished).
- [34] O. Gessner *et al.*, *Science* **311**, 219 (2006).
- [35] A. M. Rijs, M. H. M. Janssen, E. T. H. Chrysostom, and C. C. Hayden, *Phys. Rev. Lett.* **92**, 123002 (2004).
- [36] C. Z. Bisgaard, O. J. Clarkin, G. R. Wu, A. M. D. Lee, O. Gessner, C. C. Hayden, and A. Stolow, *Science* **323**, 1464 (2009).
- [37] J. G. Norman, *J. Chem. Phys.* **61**, 4630 (1974).
- [38] M. Cook, Ph.D. thesis, Harvard University, 1981.
- [39] Y. Hikosaka, J. H. D. Eland, T. M. Watson, and I. Powis, *J. Chem. Phys.* **115**, 4593 (2001).
- [40] K. Schwarz, *Phys. Rev. B* **5**, 2466 (1972).
- [41] J. C. Slater, *The Self-Consistent Field for Molecules and Solids* (McGraw Hill, New York, 1974).
- [42] V. Myrseth, J. D. Bozek, E. Kukkk, L. J. Saethre, and T. D. Thomas, *J. Electron Spectrosc. Relat. Phenom.* **122**, 57 (2002).
- [43] K. P. Huber and G. Herzberg, *Constants of Diatomic Molecules* (Van Nostrand Reinhold, New York, 1979).
- [44] M. Schmidbauer, A. L. D. Kilcoyne, H. M. Köppe, J. Feldhaus, and A. M. Bradshaw, *Chem. Phys. Lett.* **199**, 119 (1992).
- [45] C. M. Truesdale, D. W. Lindle, P. H. Kobrin, U. E. Becker, H. G. Kerkhoff, P. A. Heimann, T. A. Ferrett, and D. A. Shirley, *J. Chem. Phys.* **80**, 2319 (1984).
- [46] T. Jahnke *et al.*, *Phys. Rev. Lett.* **88**, 073002 (2002).
- [47] B. Zimmermann, K. Wang, and V. McKoy, *Phys. Rev. A* **67**, 042711 (2003).
- [48] B. Kempgens, K. Maier, A. Kivimaki, H. M. Koppe, and M. Neeb, *J. Phys. B* **30**, L741 (1997).
- [49] T. X. Carroll, K. J. Borve, L. J. Saethre, J. D. Bozek, E. Kukkk, J. A. Hahne, and T. D. Thomas, *J. Chem. Phys.* **116**, 10221 (2002).
- [50] U. Hergenhahn, *J. Phys. B* **37**, R89 (2004).
- [51] M. Matsumoto *et al.*, *Chem. Phys. Lett.* **417**, 89 (2006).
- [52] R. D. Muino, D. Rolles, F. J. G. de Abajo, F. Starrost, W. Schattke, C. S. Fadley, and M. A. Van Hove, *J. Electron Spectrosc. Relat. Phenom.* **114**, 99 (2001).
- [53] D. L. Lynch and V. McKoy, *Phys. Rev. A* **30**, 1561 (1984).